Research Repository UCD

Title	Atmospheric pressure plasma acoustic moment analysis
Authors(s)	Law, Victor J., O'Neill, Feidhlim T., Dowling, Denis P.
Publication date	2011
Publication information	Law, Victor J., Feidhlim T. O'Neill, and Denis P. Dowling. "Atmospheric Pressure Plasma Acoustic Moment Analysis." American Institute of Physics, 2011. https://doi.org/10.1063/1.3637773.
Conference details	NUMERICAL ANALYSIS AND APPLIED MATHEMATICS ICNAAM 2011: International Conference on Numerical Analysis and Applied Mathematics, 19–25 September 2011, Halkidiki, (Greece)
Publisher	American Institute of Physics
Item record/more information	http://hdl.handle.net/10197/4786
Publisher's statement	The following article appeared in NUMERICAL ANALYSIS AND APPLIED MATHEMATICS ICNAAM 2011: International Conference on Numerical Analysis and Applied Mathematics, 19–25 September 2011, Halkidiki, (Greece), : 977-980 and may be found at http://dx.doi/org/10.1063/1.3637773 . The article may be downloaded for personal use only. Any other use requires prior permission of the author and the American Institute of Physics.
Publisher's version (DOI)	10.1063/1.3637773

Downloaded 2026-05-01 23:47:43

The UCD community has made this article openly available. Please share how this access benefits you. Your story matters! (@ucd_oa)

© Some rights reserved. For more information

Atmospheric Pressure Plasma Acoustic Moment Analysis

Victor J Law
Dublin City University, National Centre of Plasma Science and Technology, Collins Avenue, Glasnevin, Dublin 9, Dublin, Ireland

Feidhlim T O'Neill
Denis P Dowling
School Mechanical and Materials Engineering, University College Dublin, Belfield, Dublin 4, Ireland

Low-order moment around the mean (mean, standard deviation and skewness) analysis of the time evolving specific acoustic intensity of an air atmospheric pressure plasma jet is performed as a function of nozzle-to-surface gap (0.5 to 7 cm), drive frequency (19, 22, and 25 kHz) and air flow rate (35.7 to 76.6 l/m). The probability distribution of each time-series dataset exhibits deterministic correlations with contrasting entropy process regions afterglow (blown arc process (gap = 0.5 cm and 1740 ±100 K); and gap = 1 to 7 cm and 300 to 400 K)). The results indicate that the heated air is channeled along the surface and has a preferred backscatter angular. In addition the blown arc process exhibits a skewness of +0.055 and the afterglow has skewness values from -0.05 to -0.4. These results illustrate how acoustic information can be used to differentiate plasma-surface entropy states.

1. Introduction

Complex systems that contain electro-mechanical and bio-mechanical elements emit characteristic acoustic noise that can be recognized by the human ear. In an attempt to automate this human sensory behaviour non-invasive acoustic metrology has attracted much interest. For example: the semiconductor manufacturing industry [1] nuclear power generation [2], plasma welding [3], environment monitoring [4, 5] and the food health sector [6]. Within this body of work multivariate analysis tools such as Principal Component Analysis and low-order moment analysis (mean, standard deviation, skewness and kurtosis) have been used to separate out the deterministic component from the stochastic (background) noise. Recently real-time non-invasive acoustic metrology, at a specific frequency, and over a given frequency range, has been applied to atmospheric pressure plasma (APP) to measure the electrical performance [7, 8], identify the APP jet nozzle, [9, 10] and generate an acoustic image of the treatment surface [10]. The ability to map the treated surface and estimate the temperature of the process has immense technological importance when processing temperature sensitive materials such as: polymers and biological materials. The impact of this technology offers enhanced quality of care at reduced cost and will be of immense societal and commercial value.

This paper examines the specific acoustic intensity at a fixed distance of 9 cm from an atmospheric pressure plasma jet (APPJ) as it is positioned over typical surfaces (ceramic and steel) that are employed within the automobile, aerospace and medical device manufacturing sectors. The analysis approach used in this paper is based on the assumption that an acoustic point-source (of finite volume) generates a time-varying signal that has a Gaussian probability distribution, and that the introduction of a deterministic component (i.e.

elongation of acoustic source volume) will alter the time-varying signal probability distribution. Linear statistical analysis of the first three orders of moments around the mean (mean, standard deviation, and skewness) are used to construct Cartesian low-order shape-space diagrams which delineate the known temperature regions between the plasma [9, 10] and the treated surface. The use of acoustic low-order moments may be considered analogous to the term 'timbre', which distinguishes source(s) of sound production of a musical tone. This approach has the additional advantage of using all the sampled time sequence data points, as compared to using a reduced dataset of extreme time series values (minimum and maximum values) of the original time series dataset as proposed by Kugiumtzis [11] and used by Charakopoulos *et al* [12] when monitoring human brain activity and turbulence in jet systems. The disadvantage using minimum and maximum approach is that up to 75% of the original dataset may be lost [12] which may impact on the discrimination potency. However it must be stated that the 3rd order of moment around the mean (skewness) needs careful interpretation as a zero skewness does not imply that the mean = median, as in the case of discrete distributions which are multimodal or have a significant Kurtosis component. Given this corollary the skewness criteria must have addition supportive evidence when used as a metrology tool.

2. APPJ and acoustic hardware

The APPJ used in this work is the pilot scale PlasmaTreat Open-Air system manufactured by PlasmaTreat GmbH. The working gas is compressed air (1000 to 3000 mbar and 35.6 to 76.6 liters per minute (l/m)). The system is electrically powered using a 19 to 25 kHz high voltage positive uni-polar square-wave pulse-width modulated power supply with an effective duty cycle of 50%. The APPJ is mounted on a computer numerically controlled gantry allowing full XYZ positioning over a treatment surface. When the APPJ is turned on, the sound pressure level increased between 90 and 103 dB at an applied dc pulse voltage of 10 kV and duty cycle of 10–100%. For full details of the APPJ, see reference [8, 9, 10, 13, and 14].

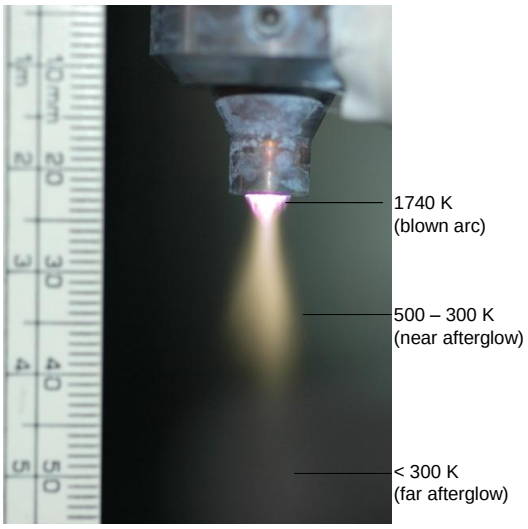

Figure 1. Photograph of Air APPJ with the N_2 rotational temperature as a function of discharge axial distance.

An Omni-directional condenser microphone positioned perpendicular to the APPJ nozzle at a distance 9 cm, acts as both a sound sensor and as a Near-field E-probe. The functional duality of the microphone

captures the electro-acoustic emission of the APPJ and converts the signals in to a convoluted analogue voltage; which in turn is passed to a Dell Precision M90 laptop computer that is fitted with a Sigma Tel Audio soundcard. The soundcard digitizes the analog signal for real-time processing using National Instruments LabVIEW software. Figure 1 provides a photograph of a 19 kHz driven air APPJ along with the nitrogen gas rotational temperature as a function of discharge axial regions; these are blown arc, and flowing afterglow (near and far regions.

The LabVIEW (version 8.2) software program samples the acoustic data over a frequency range between 0 to 25 kHz to produce a frequency spectrum with resolution of one data point per Hz. The acoustic frequency spectrum then undergoes conditioning using a Savitzky-Golay (SG) digital filter [15]. The SG filter smoothes the spectrum data points by least square minimisation with a polynomial function ($m = 1$) within a symmetrical moving window, see equation 1.

$$2k + 1, \tag{1}$$

where k are the ± sampled data points either of the interrogated data point. In this work, a k value of 10 Hz preserves the rapid rise and fall time of the electrical component (the power supply: drive signal and its harmonics) of the convoluted electro-acoustic signal and thus prevent the digital moving widow filter process over sampling according to the Nyquist-Shannon criteria [16, 17]. This approach differs from the technique of delay embedding to calculate the average mutual information (AMF) [18, 19], which in information theory is analogous to the autocorrelation function. Following on from the previous work of Law *et al* [9, 10], the frequency at which the surface provides a specific acoustic intensity (SAI) response (8 kHz) is interrogated at a sampling rate of 1 data point per 0.5 seconds as a function of both time and space. Figure 2 provides two typical APPJ time-varying SAI traces at a nozzle-to-surface gap distance of 0.5 cm and 7 cm, respectively. The electrical drive frequency is 19 kHz. For clarity only, the time-traces contain N = 300 data points with each point corresponding to a 1-second increment in time. Figure 3 depicts the probability distribution histogram for the 0.5 cm and 7 cm datasets, but over an extend time of 200 seconds. The number of bins for each dataset is determined using the $\sqrt{N}$ criteria, where N is the number of data points. Given the two types of data, representation (time-trace and probability distribution histogram) presented here; there can be seen a clear visual differentiation between the dataset that represent contrasting plasma processing applications. First, consider the two time-traces in figure 2. Both traces show no sign of periodicity but fluctuate over an amplitude span of approximately 5 dB. Second their mean SAI values are significant different (-53.6 dB for the 0.5 cm dataset and -57.8 dB for the 7 cm dataset). The mean acoustic amplitude difference (4.2 dB) is primarily due to acoustic reflection from the surface: this aspect is discussed later in the paper. Thirdly, the two histograms have a Gaussian fitted. The curves show that the 0.5 cm dataset presents a near normal probability distribution whereas the 7 cm is weighted (skewed) to lower acoustic amplitudes.

To quantify the observed differences within these datasets, and others, a metrology method needs to be introduced to; describe, compare, and contrast, the shape of the datasets. In addition, the goal of this metrology is to extract useful spatial and temperature process information. The final part of this section sets out the mathematical metrology to achieve this goal.

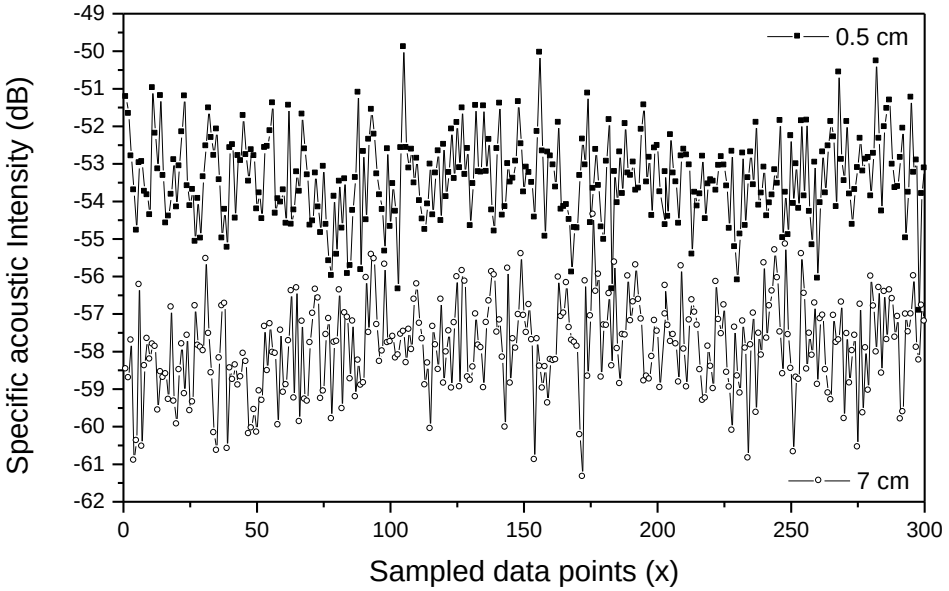

Figure 2. Typical APPJ acoustic emission time-trace (sampling period = 300 seconds). Solid-line = 0.5 cm and dashed-line = 7 cm nozzle-to-surface gap distance. Electrical drive frequency = 25 kHz.

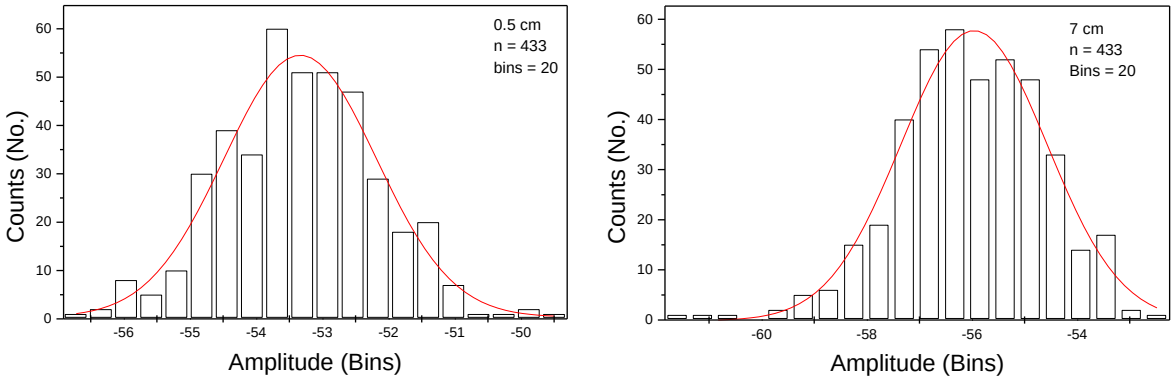

Figure 3**.** Probability distribution histograms for 0.5 cm and 7 cm nozzle-to-surface gap distance. Data points = 433 and 20 bins.

The metrology used here is based upon Low-order moment analysis of time series data of length *N*, *x*(*t*), *t* = 1,2,….*N*. This methodology is used discriminate and define the vertical surface location and process temperature by calculating the first three moments around the acoustic mean intensity. These are:

Mean (μ),

$$\mu = \frac{1}{N}\sum_{i=0}^{n-1} x_j \qquad (2)$$

Standard deviation (σ),

$$\sigma = \frac{1}{N}\sum_{i=0}^{n-1}\left(x_j - \mu\right) \quad (3)$$

and the normalized 3rd order moment ((γ_1): skewness). The value γ_1 is calculated using equations 3 and 5.

$$\gamma_1 = \frac{\mu^3}{\sigma^3} \quad (4)$$

$$\mu_x^3 = \frac{1}{N}\sum_{i=0}^{n-1}\left(x_j - \mu\right)^3 \quad (5)$$

In equation (4), μ^3 is the 3rd moment of the mean, and σ_x^3 is the standard deviation to the power of 3 of the dataset. In equation (5) μ^3 is calculated, where *N* is the number of elements (433) in the sampled time sequence x. It is important to note that a zero value indicates the distribution is relatively evenly distributed on both sides of the mean; the distribution could be bi-modal and a have a significant Kurtosis component.

3. Shape space analysis

In this work 40 time-varying SAI measurements are made with each measurement containing 433 sampled values over 216 second period. The measurements were made as follows: 20 ceramic samples at 25 kHz, 14 ceramic samples at 19 kHz and 6 steel samples at 25 kHz. The measurements are further characterized by a fixed nozzle-to-surface gap of 7 to 0.5 cm at either 1 or 0.5 cm steps intervals. Under these varying gap distance values the APPJ discharge temperature region in contact with the surface changes from far afterglow (300 to 290 K) at 7 cm, through the near afterglow at 0.5 cm to 3-4 cm (500 to 300 K), and to the blown arc region (1740 ±100 K) at 0.5 cm. In addition the microphone, incident angle reduces from 38 to 3 degrees.

Figure 4 shows the mean acoustic intensity (μ) for all 40 time-vary SAI measurements as a function of gap distance and microphone incident angle. The acoustic data has 2 nodes (1 to 3.5 cm and 4 to 7 cm) within a common μ decline as the nozzle-to-surface gap increases. The severance point (4 cm) between these nodes is associated with the visible afterglow from the surface. This phonological feature suggest that cooled ions arriving at the surface have a role, acoustic noise process as the reflected molecular gas is channeled along the perpendicular surface and with a preferred microphone incident angle of 25 to 35^o. Three further features of note are: firstly that the μ values decreases with drive frequency, second air flow rate has an effect on the acoustic level and third, the comparative ceramic and steel surface data exhibit little difference in their μ value. The use of μ as a process temperature measurement however is limited as there are multiple μ values for a given drive frequency, and air flow rate as the nozzle-to-surface varies. For example 3, 5 and 6.5 cm have similar values of μ ~ -57 dB.

In addition to this data, it is necessary to know the run-to-run and day-to-day variation in the SAI measurement. To access this information the measurement instrumentation was dismantled and rebuilt every

few weeks over a 2 month period. The total spread in collected data was found to be ±1 dB. This value is an experiment offset only and did not alter acoustic outcome. For clarity this maximum spread in μ is only shown on the first 19 kHz, 35.7 l/m data point. This day-to-day variation is used as the minimum separation to identity any deterministic effect in shape-space.

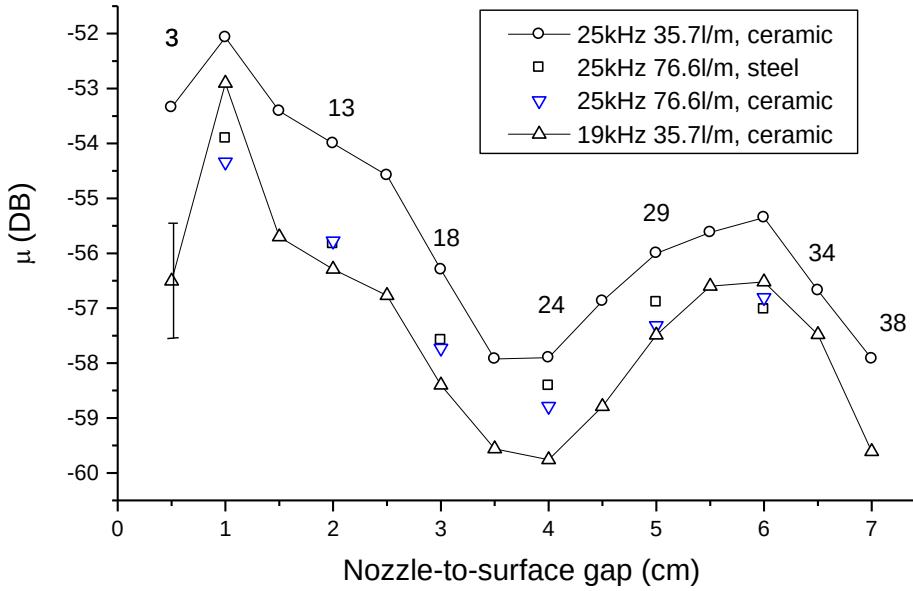

Figure 4. Specific acoustic intensity μ plotted against distance & microphone incident angle for steel and ceramic datasets.

To remove the angular distribution effect the 25 kHz, 35.7 l/m ceramic dataset has been computed for their associated σ values. These values are displayed in figure 5 within Cartesian shape-space with μ plotted on the abscissa axis and σ plotted on the ordinate axis; also included are the three plasma regions as a function gap. The shape-space reveals that the 0.5 cm arc process is separated from the remaining 13 data points. Parametric cluster analysis [20] indicates that the arc process is separated by -2.395μ (dB) 0.1114 μ (dB) from the averaged center (+) of the remaining 13 data point cluster 9, see dotted box. This separation distance is over twice the measured day-to-day variation as identify in fig 4. Using this knowledge it is reasonable to classify the arc process as a separate cluster from the remaining 13 data points. In addition the 13 data points may be classified as 2 further two sub-clusters that represent the 1st (x) and 2nd node (o); where each sub-cluster ranges between -53 to -58 μ and 1.2 to 1.3 σ; and -55.35 to -57.92 μ and 1.22 1.376 σ, respectively. In the real-world these 2 clusters correlate to the discharge plume disengaging (near afterglow) from the surface and the plume free from the surface (far afterglow).

Two additional features of note can be observed in the node data points. First, trajectory analysis reveals the data point trajectory in the second node is a reversal to that of the first node data points. Second, standardization normalization of μ by σ (i.e. μ/σ) for each cluster reveals a bifurcation of the order of 40 to 47, respectively.

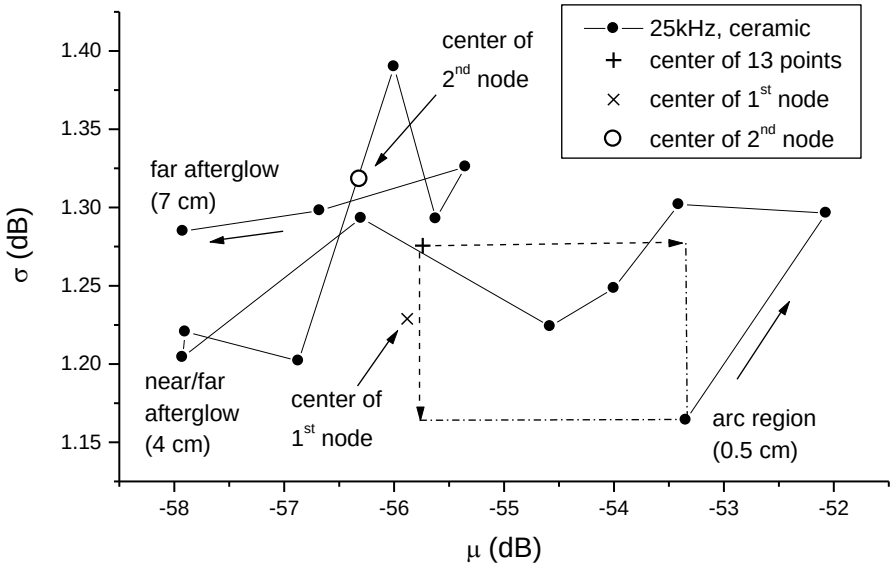

Figure 5. Specific acoustic intensity shape-space mapping (μ and σ) for 25 kHz, 35.7 l/m, ceramic dataset.

Low-order shape-space mapping (μ and σ) has also been performed on the 19 kHz, ceramic dataset and is presented in fig 6. In this case, the arc process is separated from the remaining 13 data points by 3.5 μ(dB). Here again the reversal in trajectory is initiated at the 4 cm point to produce conjugate points has an average of 0.5 μ(dB) separation. Of further note, the standardization of μ (μ/σ) within the remaining 13 data points has an average value of 40. In comparison with the 25 kHz dataset, the day-to-day separation standard (±1dB) indicates that the arc process is separated even further from the remaining data points and that the remaining points can be classified as a single cluster.

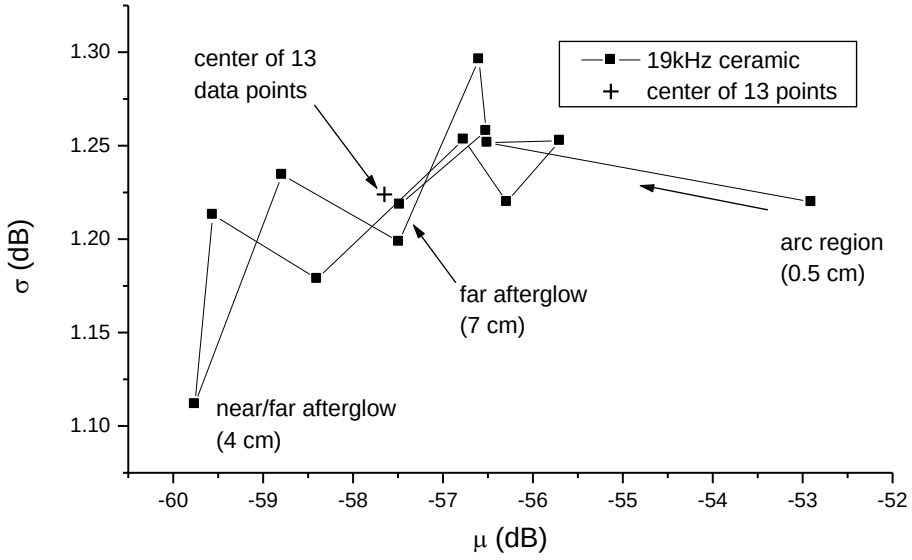

Figure 6. Specific acoustic intensity shape-space mapping (μ and σ) for the 19 kHz, 35.7 l/m, ceramic dataset.

The shape-space mapping has also been extended to μ and γ_1. Results of 2D mapping are not shown here but are described. In this case the arc process has a γ_1 ~ +0.055, or, near-Gaussian distribution implying that the reduced acoustic source volume resembles a casual pure tone. In addition, as the gap increases γ_1 becomes negative within the range of - 0.5 to -0.42, indicating a casual dependence as the acoustic source volume increases. The use of 3 low-order moments allows moment analysis to be displayed in Cartesian 3D shape-space. Figure 7 shows this display for the ceramic data using National instrument LabVIEW software, where the three axis's are labeled: X-axis = mean, Y-axis = STD, and Z-axis = Skewness. Using this software the viewing angle can be rotated in real-time for complete inspection of the shape-space. However, for this paper a fixed orthogonal view is chosen. The display reveals the start (0.5 cm arc) of the data point sequence (coordinates: μ = -0.055, σ = 1.163 and γ_1 = +0.055), and the finish point within the cluster (coordinates: μ = -57.92, σ = 1.286 and γ_1 = -0.140). The important point here is the visual separation of the clusters can be maximized by selecting the appropriate viewing angle which unavailable in the 2D projection.

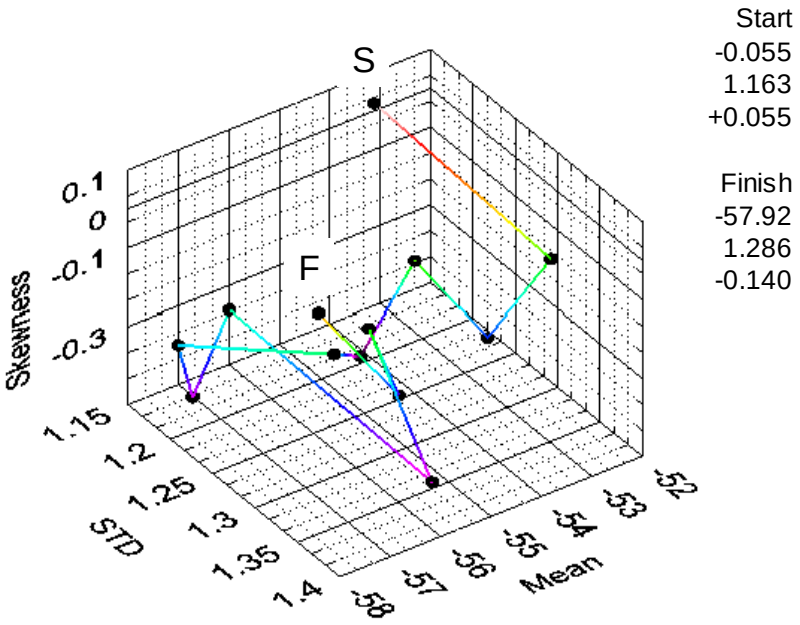

Figure 7. 3D specific acoustic intensity shape space representation of low-order values.

4. Specific acoustic intensity mapping of process parameters

The air flow and drive frequency are known to be important factors that influence plasma processing of polymers [8, 9, 10, and 19]. Figure 8 shows a triplet of acoustic intensity maps (AIM) that reveal how μ is defined by drive frequency (19, 22, 25 kHz) and helium flow at three gap distance (0.5, 3 and 7 cm). The 0.5 cm gap AIM reveals that μ varies by 5 dB across the frequency and only 2 dB across the flow parameter. Within this parameter space a flat acoustic region is produced as both flow and drive frequency is increased. This region is depicted with the letter A. Moving to the 3 cm gap AIM, the magnitude of the iso-acoustic contours decreases and change in orientation for the same parameter space: primarily due to the influence of flow rate at the higher drive frequencies (22 and 25 kHz). At the 7 cm gap distance a similar SAIM is produced to that of the 3 cm position.

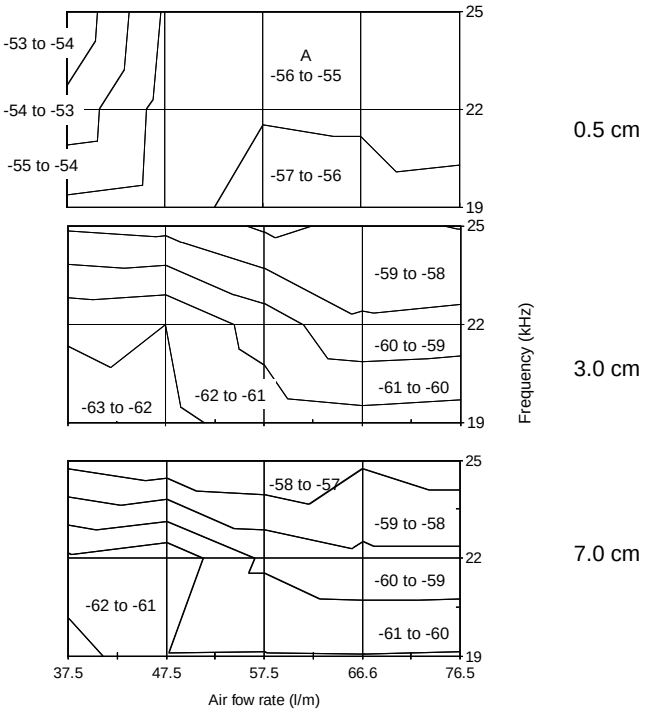

Figure 8. Triplet of specific acoustic intensity maps depicting effect of drive frequency and gas flow as a function gap distance (0.5, 3, and 7 cm) upon mean acoustic intensity.

5. Conclusions

This paper has considered time evolving specific acoustic intensity at 9 cm from air atmospheric pressure plasma jet as a function of nozzle-to-surface gap (0.5 to 7 cm). The analysis computes the low-order moments of the acoustic signal (mean, standard deviation and skewness) and displays the results in Cartesian shape-space followed by parametric cluster analysis. In addition 3D specific acoustic intensity maps are constructed to follow the APPJ as a function gas flow, drive frequency and nozzle-to-surface gap. The analysis reveals a deterministic link within μ, σ and γ_1 of the APPJ time-varying SAI signal as the gap distance is varied. Under blown arc contact conditions (i.e. reduced volume ~1 cm^3 and maximum temperature) the ASI signal is found to exhibit a pure tone that approaches maximum intensity. As the nozzle-to-surface gap increases, along with the acoustic volume (1 to 20 cm^3), the SAI mean value reduces in a bimodal manner along with an increase in negative magnitude of skewness. Comparative surface material experiments between steel and ceramic reveal that there is no significant difference in the acoustic measurement. Two-D shape-space (μ, σ) yields data clusters that are correlated to contrasting entropy plasma process regions (blown arc and flowing afterglow), and associated plasma-surface reaction temperatures. The standardization of μ reveals a bifurcation in the 25 kHz, 35.7 l/m dataset as compared to the 17 kHz, 35.7 l/m conditions. The data suggest that there is a casual relationship between the bifurcation and drive frequency. Three-D shape-space, where all low-order moments are used, a further enhancement of the projected shape can be gained. The application of SAIM translates the low-order moments into the real-world parameter-space that can be ready employed in understanding the implications of the acoustic measurement.

In this work a symmetrical moving window is used to improve the signal-noise-ratio. However, the use of an asymmetric moving widow that mimics a sound attack-sustain-release profile of the original sound signal may increase feature discrimination within the low-order moment analysis. This feature is now being investigated.

Acknowledgements

This work is supported by Science foundation Ireland 08/SRC/I1411. We would also like to thank Prof. N. Thornhill (Imperial College London, UK) and Dr. N Vevtic (Bloomsburg University, USA) for helpful discussions regarding this work.

References

[1] M Yasaka, M Takeshita, R Miyagawa. Japn. J. Appl. Phys. 39, L1268-L1288, 2000.

[2] T Biserna, F Cavallini, S Taglienti and V Tosi. Progress in Nuclear Energy. 1(2-4), 517-526. 1977.

[3] Y Wang, and P Zhao. Pressure vessels and piping. 78, 43-47, 2001.

[4] I G Rees and C G Don. J. Phys. E: Sci. Instrum. 16, 832-835, 1983.

[5] H Wu, M Siegel, and P Khosla. IEEE Trans, Instrum, measurem. 48(5), 1005-1009, 1999.

[6] A Zdunek, D Konopacka, and K Jesionkowska. J. Texture Studies. 41, 75-91, 2010.

[7] J Tynan, V J Law, P Ward, A M Hynes. J Cullen, G Byrne, D P Dowling, and S. Daniels. PSST, 19, 015015, 2010.

[8] D P Dowling, F T O'Neill, S J Langlais, and V J Law. Plasma Polymer Processing. 8(6), 718-728, 2011.

[9] V J Law, F T O'Neill and D P Dowling. PSST. 20(3), 035024, 2011.

[10] V J Law, D P Dowling, J L Walsh, F Iza, N B Janson, and M Kong. CHAOS2010: 4th Chaotic modeling & simulation international conference. Agios Nickolaos, Crete, Greece. 31st May - 3rd June 2011. Book of abstracts, pp75.

[11] D Kugiumtzis, A Papana, A Tsimpiris, I Vlachos, and P G Larsson. Time series feature evalyation in discriminating preictal EEG states. Lecture Notes in Computer Science , 4345, 298-310, 2006.

[12] A Charakopoulos, T E Karakasidis, and P Papanicolaou. 4th Chaotic Modeling and Simulation International Conference. Chaos 2011, Agios Nickolaos, Crete, Greece. 31st May - 3rd June 2011. Book of abstracts, pp56

[13] Y Kubota, R Ichiki, and T Hara, N Yamaguchi and Y Takemura. J Plasma Fusion Res. 8, 740-74. 2009.

[14] J Pulpytel, V Kumar, P Peng, V Micheli, N Laidani, and F Arefi-Khonsari. Plasma Polymer Processing. 8(6), 644-675, 2011.

[15] A Savitzky, and M J Golay. Analitical chemistry 36(8), 1627-2639. 1964.

[16] N Nyquist. Trans. AIEE 47, 617-44, 1928.

[17] S E Shannon. Proc. Inst. Radio Eng. 37, 10-21, 1949.

[18] J L Walsh, F Iza, N B Janson, V J Law and M G Kong. J Phys D: Appl. Phys. 43(7), 075201, 2010.

[19] N Jevtic, J S Schweitzer, and P Stine. Chaos Theory: Modeling, Simulation and Applications, edited by C. H Skiadas and Dimotikalis. World Scientific Publishing, 2010, pp191-199.

[20] V J Law, J Tynan, G Byrne, D P Dowling, and S Daniels. Chaos Theory: Modeling, Simulation and Applications, edited by C. H Skiadas and I Dimotikalis. World Scientific Publishing, 2010, pp147-154.